Size Distribution and Intermolecular Interaction of Laminin-1 in Physiological Solutions

Kazuo Onuma* and Noriko Kanzaki

Institute for Human Science & Biomedical Engineering, National Institute of Advanced Industrial Science and Technology, Central 6, 1-1-1 Higashi, Tsukuba, Ibaraki 305-8566, Japan

Received: June 2, 2003; In Final Form: July 23, 2003

The diffusion coefficient and hydrodynamic radius of laminin-1 (LN-1) in aqueous solutions were investigated by using a dynamic light scattering (DLS) technique. The autocorrelation functions could be analyzed assuming two relaxation modes, fast and slow, with exponential decay. We primarily focused on the fast mode, because the mass of it represented 99% of the total mass. The unit corresponding to the fast mode had a hydrodynamic radius of 20.6 ± 0.5 nm in both tris- and MOPS-buffered solutions of 150 mM NaCl and pH 7.2 at 25 °C. Intermolecular interactions between these essential units were attractive, and the Hamaker constant in tris-buffered solution was estimated as 5.2 k_BT according to DLVO theory. When the magnesium was added to the tris-buffered solutions, the attractive force strongly increased with increasing magnesium concentration. This change was not explained by the charge-screening effect of magnesium ions in the framework of the classical DLVO model.

Introduction

Laminins are representative extracellular matrix proteins that play important roles in various cell behaviors such as differentiation, growth, adhesion, and migration in vivo. Within the laminin family, laminin-1 (LN-1) was first discovered and has been investigated by many researchers to clarify its role in cellular organization.[1−10] These investigations found that LN-1 took the form of hetero-trimers with three different polypeptide chains: α (400 kD), β (220 kD) and γ (200 kD).[11] These chains are thought to be arranged in cruci-shaped LN-1 molecules of molecular weight, 820 kD, and the relationship between the form of molecules and various functions of LN-1 has received much attention. The effect of divalent cations such as calcium and magnesium on an intermolecular interaction of LN-1 has also become an interesting topic. [12−14]

The cruciform of LN-1 has been observed using electron microscopy with either positive or negative staining of samples onto a support plate.[15,16] Because the staining methods were performed under conditions far from physiological pH, it has been a concern whether the original three-dimensional form of LN-1 was conserved or not. Damage to samples by electron radiation is another problem to be considered. To overcome these problems, Chen et al. recently used atomic force microscopy (AFM) to observe LN-1 molecules.[17] They confirmed the cruciform shape of LN-1 deposited on a mica plate both in tris- and MOPS-buffered solutions. However, they also pointed out that the arm of the LN-1 molecule was flexible and moved dynamically, which changed the conformation of LN-1 widely.

The observations described above are all indirect, and to our knowledge, in situ investigation of LN-1 conformation in the solutions has not been reported. The intermolecular interaction under physiological conditions has also not been clarified, although it is known to be the most important factor to control the protein assembly. Various techniques are applicable to investigation of proteins in solutions, such as X-ray diffraction and nuclear magnetic resonance. Among these techniques, dynamic light scattering (DLS) is very convenient and widely used.[18−23] This technique provides information concerning the conformation of proteins through the diffusion coefficient and hydrodynamic radius of molecules. Moreover, intermolecular interactions can also be estimated through the relationship between the concentration of proteins and diffusion coefficient. The present study used DLS to investigate LN-1 in the solutions. We focused on size distribution of LN-1, intermolecular interaction, and the effect of a divalent cation (i.e., magnesium) on the intermolecular interaction in a tris-buffered solution. The size distribution in a MOPS-buffered solution was also measured for comparison.

Experimental Section

1. LN-1 Samples and Solutions. LN-1 purified from EHS sarcoma was purchased from SIGMA. The original solution was frozen and contains 1 mg/mL LN-1, 150 mM NaCl and 50 mM tris at pH 7.2. The frozen solution was gently melted in ice to avoid gelation. To dilute the original solution, 150 mM NaCl and 50 mM tris-HCl buffered solution at pH 7.2 were prepared. In the case of MOPS solution, the concentration of MOPS was set to 20 mM with the same concentration of NaCl and pH as the tris solution, which was a similar condition to that used in previous AFM work.[17] The pH was adjusted using 1N NaOH. The original tris solution was dialyzed to form a MOPS solution at 4 °C by using a dialysis cassette (PIERCE, USA). The concentration of LN-1 both in the tris and MOPS solutions changed from 0.05 to 0.75 mg/mL. All solutions were filtered with a 0.45-μm pore-sized filter using a centrifuge before inserting them in the DLS apparatus. The temperature of the solution at DLS measurements was set to 25 °C.

2. DLS Measurements. The DLS measurements were performed using a DLS-7000 optical system (Otsuka Electronics Co., Ltd., Osaka, Japan) with an Ar^+ laser (Spectra-Physics Lasers, Mountain View, CA) at a wavelength of 488 nm and using an ALV-5000/E correlation system (ALV−Laser Vetrie-

* To whom correspondence should be addressed. Tel.: +81-29-861-4832. Fax: +81-29-861-6149. E-mail: k.onuma@aist.go.jp.

10.1021/jp0355298 CCC: $25.00
Published on Web 09/25/2003

bsgesellschaft). The laser power was varied from 20 to 500 mW to keep the average scattering intensity above 30 000 cps in each measurement. The angular dependence on the autocorrelation functions at the scattering angles, 20−90°, with the step of 10° was observed in all measurements to clarify that the measured diffusion coefficient was really translational. Several models were tested in order to fit the autocorrelation data, such as an exponential function including different relaxation modes, a stretched exponential function with nonexponential decay, and conventional CONTIN analysis.

3. Electrophoretic Light Scattering. Surface potential (zeta potential) of an LN-1 molecule was measured by an ELS-6000H (Otsuka Electronics Co., Ltd., Osaka, Japan) with a 10 mW He−Ne laser. The average voltage per unit distance and the current were set at −40 V/cm and −44 mA, respectively. All measurements were performed on the tris-buffered LN-1 solutions (0.5 mg/mL concentration) with and without magnesium at a scattering angle of 13°. The measurements were repeated more than three times in each condition, and the data were then averaged.

Principle of Data Analysis

1. DLS. In regards to DLS measurements, the autocorrelation function, $g^{(2)}(q,t)$ and scattering vector, q, are defined as follows:

$$g^{(2)}(q,t) - 1 = \frac{\langle I(q,t)I(q,0)\rangle}{\langle I(q,0)\rangle^2} \tag{1}$$

$$q = \frac{4\pi n}{\lambda_W}\sin\left(\frac{\theta}{2}\right) \tag{2}$$

where $I(q, 0)$ and $I(q, t)$ are scattered intensities at time zero and t, t is the delay time between photon-counting measurements, n is the refractive index of the solution, λ_w is the wavelength of the laser light (i.e., 488 nm), and θ is the scattering angle. The term $g^{(2)}(q,t)$ was fitted by using the following exponential function:

$$g^{(2)}(q,t) - 1 = \left\{\sum_i K_i \exp\left(-\left(\frac{t}{\tau_i}\right)^{\beta}\right)\right\}^2 (i = 1, 2, 3 \ldots) \tag{3}$$

where τ_i is the decay time and K is a constant. Parameter β varies from 0 to 1. When $\beta = 1$, normal exponential decay occurs, and when $\beta < 1$, so-called stretched exponential type decay (which is frequently observed in a polymer solution close to the sol−gel and glass transition regions) occurs. The measured decay time τ is related to the mutual translational diffusion coefficient, D, and q^2 as $1/\tau = q^2D$. In general, D is affected by the interaction between scattered particles as

$$D = D_0\{1 + \lambda\phi + O(\phi^2) + \ldots\} \tag{4}$$

where D_0 is the real translational diffusion coefficient extrapolated to a concentration of zero, ϕ is the volume fraction, and λ indicates the magnitude and sign of the interaction between scattered particles. D_0 is converted to the hydrodynamic radius, r_H, by using the Einstein-Stokes relationship given by the Boltzman constant, k_B, temperature, T, and solvent viscosity, η, as

$$D_0 = \frac{k_B T}{6\pi\eta r_H} \tag{5}$$

The volume fraction ϕ is related to protein concentration, C, through molecular weight and the radius of a particle that is assumed to be equal to r_H.

2. Interparticle Interaction Potential. Dejaguin-Landau-Verwey-Overbeek (DLVO) theory[24] is applied to analyze interparticle interactions. Three kinds of potentials are taken into account in the present study, hard-sphere potential U_h, repulsive screened Coulomb potential U_{es}, and attractive van der Waals potential U_{vdw}. Calculated interaction parameter λ is expressed using the integral equations[25] in DLVO theory that relate the radial distribution function $g(r)$ of scattered particles.[26,27] The function $g(r)$ is expressed as

$$g(r) = \exp\left(\frac{-U(r)}{k_B T}\right) \tag{6}$$

where $U(r) = U_h + U_{es} + U_{vdw}$. Each potential is defined as follows:[28−30]

$$U_h = \infty \text{ for } r < 2a, \text{ and } 0 \text{ for } r > 2a \tag{7}$$

$$U_{es} = \frac{\epsilon a \Psi_0^{\,2}}{8\pi}\ln(1 + \exp(2a\kappa - \kappa r)) \tag{8}$$

$$U_{vdw} = -\frac{A_H}{12}\left(\frac{4a^2}{r^2 - 4a^2} + \frac{4a^2}{r^2} + 2\ln\left(\frac{r^2 - 4a^2}{r^2}\right)\right) \tag{9}$$

where a is the radius of particle, ψ_0 is the surface potential, ϵ is the dielectric constant of the solvent, κ is the screening parameter, and A_H is the Hamaker constant. Parameter κ is related to Avogadro's number, N_A, the number concentration of the ith ion, n_i, elemental charge, e, and ion valence z_i as

$$\kappa^2 = \frac{N_A e^2}{\epsilon k_B T}\sum_i n_i z_i^{\,2} \tag{10}$$

and ψ_0 is written using the charge on a particle, Z, as

$$\Psi_0 = \frac{Ze}{\epsilon a(1 + \kappa a)} \tag{11}$$

Results

1. Autocorrelation Functions of LN-1 in Tris and MOPS Solutions by DLS Measurements. Figure 1a shows $g^{(2)}(q,\tau)$ for the tris solution at two representative scattering angles, $\theta =$ 20° and 90°, with LN-1 concentration of 0.70 mg/mL. The number of data points in autocorrelation functions is reduced by one-third for clarity. Under the assumption of a representative relaxation process, single-exponential function, inserted in the figure as a dotted line, cannot fit the data at both scattering angles. However, under the assumptions of two major relaxation processes (fast and slow modes) and the use of a double-exponential function, the data is well fitted as shown by the solid line in the figure. The β value changes slightly with scattering angle. For the fast mode, β ranges from 0.95 to 1.0, and for the slow mode, 0.89−0.95. We think that the deviations of β from unity are very small and can be negligible, especially for the fast mode. Hereafter, we therefore analyze the autocorrelation function data by assuming a normal exponential decay with two relaxation modes. To check whether this analysis is appropriate or not, we also used CONTIN analysis as shown in Figure 1b. Two peaks in decay time can be seen both at $\theta =$ 20° and 90°. Because the decay times of fast and slow modes are close, the profile sometimes has a single peak with a wide

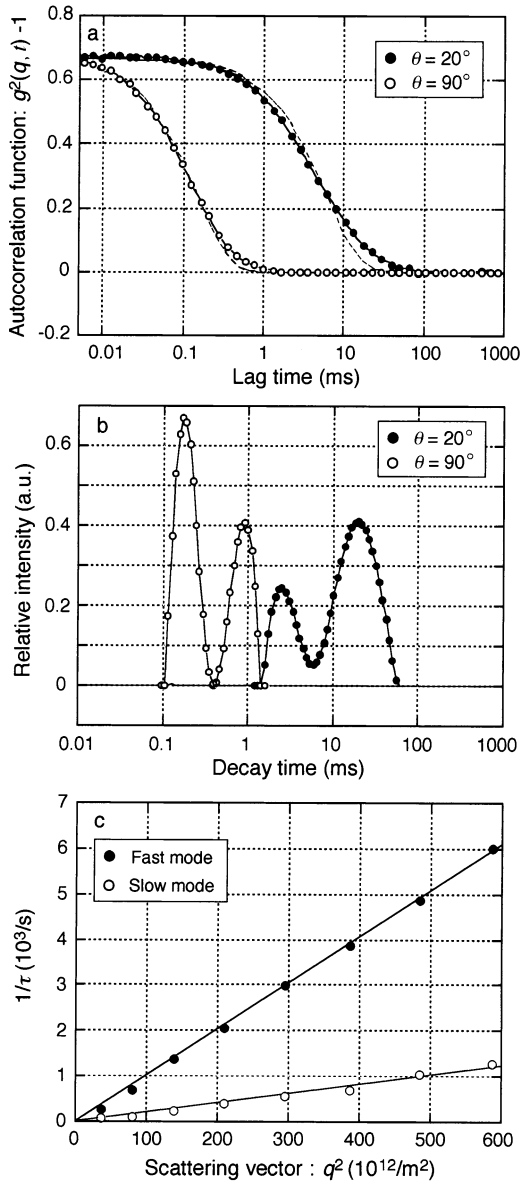

Figure 1. (a) Autocorrelation functions at $\theta = 20$ and 90° in tris solution with 0.70 mg/mL of LN-1. Solid line shows double exponential fitting, and dashed line, single-exponential fitting. (b) Distribution of decay time analyzed by CONTIN at $\theta = 20$ and 90°. (c) Relationship between $1/\tau$ and q^2.

distribution. Figure 1c shows the relationship between $1/\tau$ and q^2 based on the double-exponential analysis for a 0.70 mg/mL tris solution. Linear relationship, with the lines passing through the origin, can be seen both for fast and slow modes. Using the slopes of the lines in Figure 1c, we calculated D to be 10.2×10^{-12} m^2/s for fast mode and 2.1×10^{-12} m^2/s for slow mode. The error in each D was approximately $\pm 2-3\%$ of the measured value. D was converted to the apparent hydrodynamic radius, r_A, by using the Einstein-Stokes equation after correcting for the viscosities of the buffer solutions. At 0.70 mg/mL LN-1, the calculated r_A was 23.6 nm for fast mode and 115 nm for slow mode. Although the contributions to the total scattering intensity from each mode are comparable (Figure 1b), the weight of the scatterer for the fast mode was much higher than that for the slow mode. The relative mass distribution of particles associated with each mode can be estimated from the following relationship:

$$I(\theta) = KM\mathrm{w}CP(\theta) \tag{12}$$

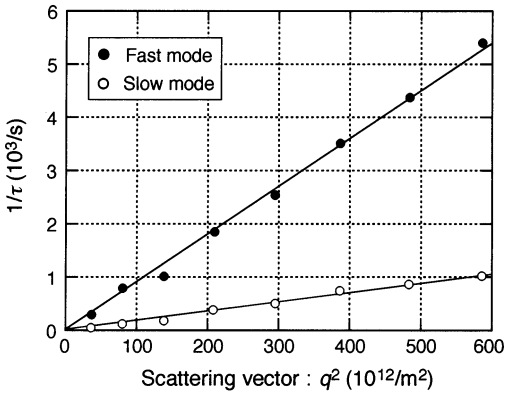

Figure 2. Relationship between $1/\tau$ and q^2 in MOPS solution with 0.65 mg/mL of LN-1.

where $I(\theta)$ is the intensity at scattering angle, θ, and K, Mw, C, and $P(\theta)$ are the optical constant, molecular weight, concentration of each scatterer, and interference factor, respectively. Constant $P(\theta)$ is written using x as

$$P(\theta) = (3x^{-3}(\sin x - x \cos x))^2 \tag{13}$$

$$x = \frac{4\pi r_A}{\lambda_W} \sin\left(\frac{\theta}{2}\right) \tag{14}$$

Because Mw is proportional to $r_A{}^3$, $I(\theta)/C$ is proportional to $r_A{}^3P(\theta)$. Conversion from the distribution of scattering intensity, $G(d)$ to that of mass, $W(d)$, is therefore

$$W(d) = \frac{G(d)}{8r_A{}^3P(\theta)} \tag{15}$$

From the ratio of fast and slow modes seen in Figure 1b, we found that the fast mode scatterers represented approximately 99% of the total mass.

In regards to the MOPS solution, the same procedure as outlined above was done for the autocorrelation data set. Under the assumption of exponential decay, two relaxation modes were found to be applicable, as was the case for the tris solution. Figure 2 shows the relationship between $1/\tau$ and q^2 for a 0.65 mg/mL LN-1 solution. The parameter D is 9.1×10^{-12} m^2/s for fast mode and 1.8×10^{-12} m^2/s for slow mode. These values are 10−20% smaller than those estimated in the case of the tris solution. The parameter r_A was calculated as 26.2 nm for fast mode and 133 nm for slow mode.

According to the estimated r_A, fast mode corresponds to the monomer of LN-1 molecule, and slow mode, the aggregate of LN-1 molecules. Hereafter, we focus on the behavior of fast mode.

2. Dependence of Diffusion Coefficient on LN-1 Concentration in Tris and MOPS Solutions. The two relaxation modes observed at 0.70 mg/mL concentration of LN-1 were also confirmed at other concentrations. Figure 3 shows the relationship between D for fast mode and the volume fraction of LN-1 in tris and MOPS solutions. It is clear that D linearly decreases with increasing concentration in both solutions. However, the decrease rate is approximately two times faster in the MOPS solution than in the tris solution. Estimated D_0 was 11.5×10^{-12} m^2/s for the tris solution. This value corresponds to a real hydrodynamic radius, r_H, of 21.0 nm. In the MOPS solution, D_0 for fast mode was calculated to be 11.8×10^{-12} m^2/s, and r_H was 20.3 nm. The differences in D_0 and r_H in the case of the tris and MOPS solutions are in the error

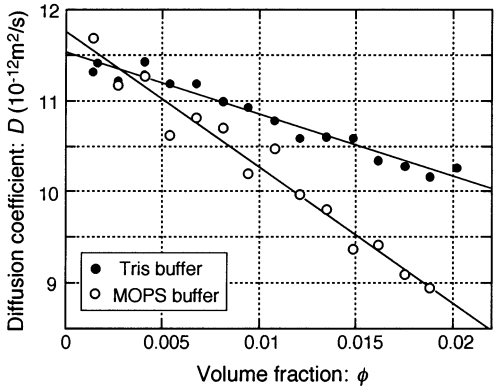

Figure 3. Relationships between diffusion coefficient and volume fraction of LN-1 in tris (open symbols) and MOPS (solid symbols) solutions.

range (of ±2−3%), thus, the conformation of LN-1 monomer can be considered to be the same in both solutions.

3. Effect of Mg^{2+} on the Relationship between Diffusion Coefficient and LN-1 Concentration in Tris Solutions. The divalent cations, especially Ca^{2+} and Mg^{2+}, were found to greatly affect the aggregation of LN-1 revealed through the previous turbidity measurements.[12−14] Although it was found that Ca^{2+} had a greater effect on aggregation than Mg^{2+}, it has not been clarified how the intermolecular interaction changes with the concentration of each cation. Accordingly, we performed measurements of diffusion coefficients in relation to LN-1 concentrations under various cation concentrations. We first tested the effect of Ca^{2+}; however, it was found that the aggregation process quickly proceeded, and no reliable data of autocorrelation functions could be obtained. Thus, in the present study, we only investigated the effect of Mg^{2+}, which was added as $MgCl_2$ to the LN-1 solutions in concentrations from 0.1 to 5 mM. At first, the size distribution of particles in the presence of Mg^{2+} was investigated. Figure 4a shows an example of the autocorrelation functions at $\theta = 20$, 50 and 90° for a 0.7 mg/mL LN-1 solution in the presence of 1 mM of Mg^{2+}. As in the case of the Mg^{2+} free solution, the autocorrelation function data can be analyzed by assuming two relaxation modes in the solution. Figure 4b shows the relationship between $1/\tau$ and q^2. The apparent diffusion coefficients for fast and slow modes are 9.7×10^{-12} m^2/s and 2.2×10^{-12} m^2/s, respectively. The measurements with changing the concentration of LN-1 indicate that the essential form of fast mode in the presence of Mg^{2+} is the same as that in Mg^{2+} free solutions. It should be noted that the plotted data of $1/\tau$ and q^2 tend to disperse in the case of 5 mM of Mg^{2+}, probably owing to the strong interaction described below.

Figure 5 shows the relationship between D/D_0 of fast mode and LN-1 volume fraction in the presence of 0.1, 1, and 5 mM of Mg^{2+}. For reference, the data obtained without Mg^{2+} is also plotted. In all cases, D/D_0 decreased linearly as the concentration of LN-1 increased, and the decrease rate increased with the concentration of Mg^{2+}. Below 0.1 mM of Mg^{2+}, the relationship between D/D_0 and LN-1 volume fraction was almost the same as that in Mg^{2+} free solution. Equation 4 was used to calculate λ values in all concentrations of Mg^{2+}, and λ is plotted as a function of Mg^{2+} concentration in Figure 6. This figure shows that λ decreases steeply with increasing concentration.

2. Electrophoretic Light Scattering Measurement in Tris Solution. The results of measurements by electropholetic light scattering are shown in Figure 7. In the case of a Mg^{2+} free solution, the zeta potential of particles was found to be a

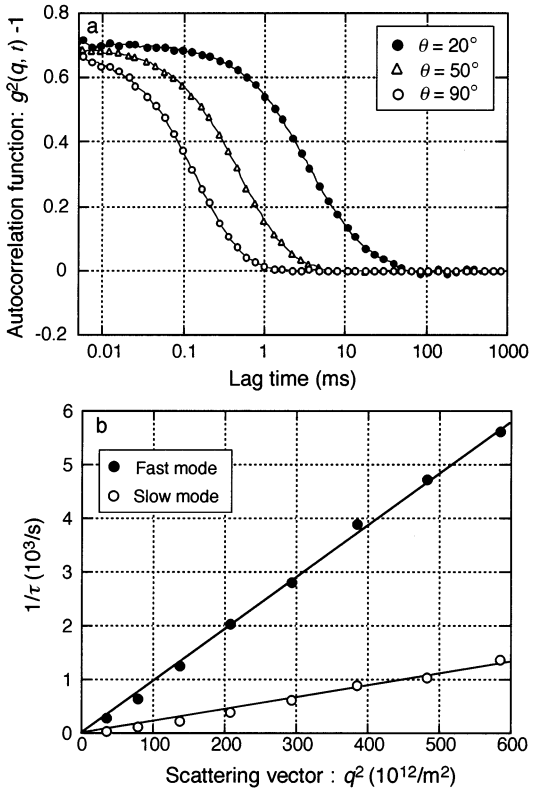

Figure 4. (a) Autocorrelation functions at $\theta = 20$, 50 and 90° with 0.7 mg/mL LN-1 solution in the presence of 1 mM of magnesium. Data are fitted by double exponential functions. (b) Relationship between $1/\tau$ and q^2.

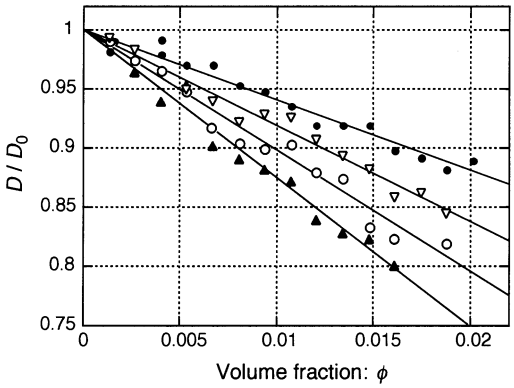

Figure 5. Relationship between D/D_0 and volume fraction of LN-1 depending on concentration of magnesium. Magnesium concentrations are zero (solid circles), 0.1 (reverse open triangles), 1.0 (open circles), and 5 mM (solid triangles).

negative value, -7.7 ± 0.3 mV. With the addition of magnesium to the solution, zeta potential changes toward neutral as shown in the figure. That is, it changes gently up to 1 mM of Mg^{2+} and increased quickly between 1 and 3 mM. Around 5 mM of Mg^{2+}, zeta potential reaches a maximum of -4.4 ± 0.5 mV.

Discussion

First, we discuss the conformation of LN-1 molecules in physiological solutions. As described in the Introduction, an LN-1 molecule is composed of three hetero proteins forming a cruciform, and the length of each arm was estimated as 36 nm for three short arms and 77 nm for one long arm. When this form is completely held in the solutions, the LN-1 monomer has a fairly anisotropic form, and its hydrodynamic radius should exceed 30 nm under the assumption of a simple solid sphere.

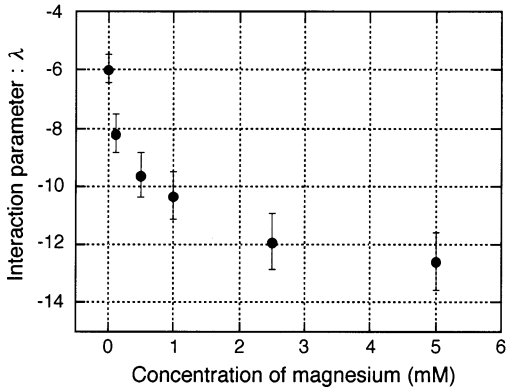

Figure 6. Change in interaction parameter, λ, depending on magnesium concentration.

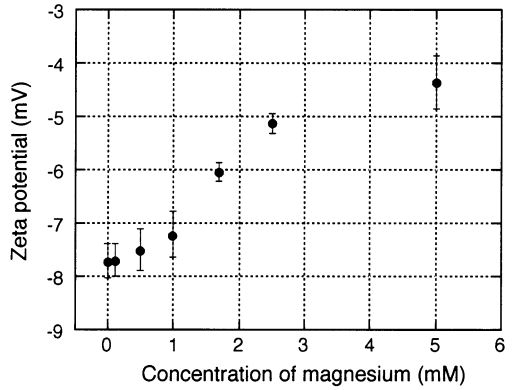

Figure 7. Change in zeta potential of LN-1 molecules depending on magnesium concentration.

However, our DLS measurements showed the radius as 20−21 nm under the present conditions, and these values are much smaller than that expected from the complete cruciform of LN-1. Moreover, we could not observe depolarized scattering (vh-scattering) in LN-1 solutions. When a protein molecule or aggregates had anisotropy in their morphology or in internal bonding, depolarized scattering, which depends on the degree of anisotropy, could be measured as shown in our previous study of a bc_1-complex membrane protein. Taking these observations into account, we think that each arm of an LN-1 molecule is bent flexibly and the molecule takes a compact form in the present solutions.

On the other hand, the size (decay time) distribution determined by CONTIN analysis (Figure 1b) indicates polydispersity of particles of the fast mode. Second-order cumulant fitting for the fast mode shows that the polydispersion index is larger than 0.3. This suggests that LN-1 monomers can take several forms, although the major form in the present solutions is a compact one with flexibly bent arms. Thus, complete cruciform with open arms is probable despite the small amount of this form. This result is consistent with the previous AFM observations under similar conditions to those used in the present experiments. Chen et al. showed that the conformation of LN-1 monomer changes widely from a complete cruciform to a sphere-like form depending on the concentration of salt and the kind of buffers.[17] Especially in a high salt tris-buffered solution, LN-1 frequently took a compact form. Our DLS measurements are in accordance with their observations.

We next discuss the intermolecular interaction between LN-1 monomers and its change with the addition of magnesium. First, we assume competition of two kinds of interactions in order to analyze the data in Figure 5; namely, repulsive electrostatic

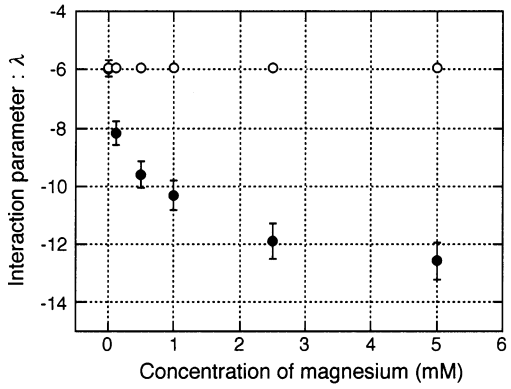

Figure 8. Change in calculated λ depending on magnesium concentration (open circles) when $A_H = 5.2\ k_BT$ and $Z = 20$. Note that λ values are constant and independent of concentration. Solid circles are measured values as a reference.

interaction from U_{es}, and attractive van der Waals interaction from U_{vdw}, as described earlier. When magnesium was not in the solution, λ was −6.0. Calculating DLVO integral equations by using the zeta potential, which is assumed to be equal to ψ_0 in eq 11, gives the Hamaker constant, A_H, as 5.2 k_BT. Moreover, Z in eq 11 is calculated as 20 from the value of ψ_0. This A_H is fairly large compared to that of bc_1-complex (M. W. = 240 kD), 0.3−1.0 k_BT, despite the fact that Z values are comparable in both cases.[31] It was reported that A_H in large molecular weight proteins, except a bc_1-complex, such as α-Crystallin (M. W. = 800 kD)[32] and apoferritin (M. W. = 440 kD),[23] are also small, approximately in the order of k_BT. We think that this difference between A_H of LN-1 and other large molecular weight proteins is naturally expected from the fact that extracellular matrix proteins, such as LN-1, should construct an oligomer or bridges (or both) between molecules to physically support the organization structures in vivo.

The change in λ when magnesium is added in the solution is estimated by using the parameters obtained above. The result is shown in Figure 8. If we assume a classical DLVO model including the competition between U_{es} and U_{vdw}, calculated λ from A_H and Z are almost constant independent of magnesium concentration. Several authors have reported such non-DLVO type interaction.[33−35] Representative forces that induce non-DLVO effect are hydration force and hydrophobic interaction. The former is caused by water structuring around protein molecules and is repulsive in nature. The origin of the later is not clarified in detail, but is attractive in nature. Another cause of non-DLVO are the so-called "salt specific" or "salt bridging" effects, which are both attractive. These forces or effects are all chemically induced. On the other hand, a physical force that induces non-DLVO interaction is an attractive depletion interaction by osmotic pressure of a polymer in buffer solutions. Poly(ethylene glycol) is representative to induce this effect.

Among the above forces and effects concerning an increase in attractive force, we believe that salt specific or salt bridging effects can sufficiently explain the result in Figure 8. This is because the surface charge on LN-1 should be changed with addition of magnesium to the solution. Figure 9 plots ψ_0 values calculated using $Z = 20$ against magnesium concentration (open circles in the figure). This figure clearly shows a large discrepancy between calculated and measured values. To make the calculated ψ_0 coincide with the measured one, Z should be decreased from 20 to 12 as increase in magnesium concentration (open triangles in figure). We thus conclude that the effect of magnesium is not simple charge screening near the LN-1 surface but the formation of bonding or adsorption on LN-1 molecules.

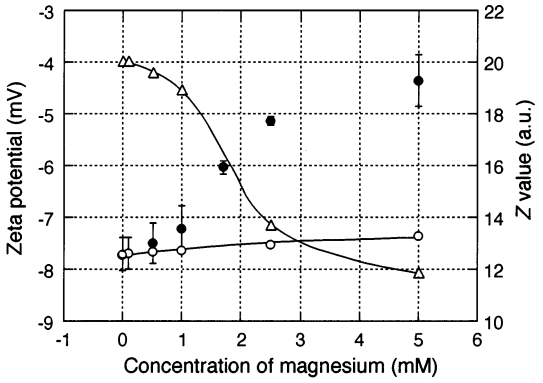

Figure 9. Change in calculated zeta potentials depending on magnesium concentration (open circles). The change is much smaller than that for measured values (solid circles). To make the calculated values coincide with the measured ones, *Z* should be decreased from 20 to 12 as magnesium concentration increases (open triangles). Curves are guides for the eye.

This behavior of magnesium for LN-1 may be comparable to the salt bridging observed in several proteins. Zinc for insulin and cadmium for apoferritin are good examples of this behavior. Both ions increase the attractive force and bind each molecule like a bridge, following the formation of an aggregate. Although clear oligomerization of LN-1 in the presence of magnesium was not observed in the present study, we think that magnesium is strongly related to the formation of aggregate via a similar effect to salt bridging, which is consistent to the results obtained in the previous turbidity measurements.

Acknowledgment. This study was supported by the Agency of Industrial Science and Technology (AIST).

References and Notes

(1) Beck, K.; Hunter, I.; Engel, J. *FASEB J.* **1990**, *4*, 148.
(2) Rizzino, A.; Terranova, V.; Rohrbach, D.; Crowley, C.; Rizzino, H. *J. Supramol. Struct.* **1980**, *13*, 243.
(3) Johansson, S.; Kjellen, L.; Hook, M.; Timpl, R. *J. Cell Biol.* **1981**, *90*, 260.
(4) Engel, J.; Odermatt, E.; Engel, A. *J. Mol. Biol.* **1981**, *150*, 97.
(5) Timpl, R.; Engel, J.; Martin, G. R. *Trends Biochem. Sci.* **1983**, *8*, 207.
(6) Manthorpe, M.; engvall, E.; Ruoslahti, E.; Longo, F.; Davis, G.; Varon, S. *J. Cell Biol.* **1983**, *97*, 1882.
(7) Terranova, V.; Rao, C.; Kalebic, T.; Margulies, I.; Liotta, L. *Proc. Natl. Acad. Sci. U.S.A.* **1983**, *80*, 444.
(8) Kleinman, H.; Cannon, F.; Laurie, G.; Hassell, J.; Aumailey, M.; Terranova, V.; Martin, G.; DuBois-Dalcq, M. *J. Cell. Biochem.* **1985**, *27*, 317.
(9) Martin, G.; Timpl. R. *Annu. Rev. Cell Biol.* **1987**, *3*, 57.
(10) Timple, R.; Brown, J. *Matrix Biol.* **1994**, *14*, 275.
(11) Burgeson, R. E.; Chiquet, M.; Deutzmann, R.; Ekblom, P.; Engel, J.; Kleinman, H.; Martin, G. R.; Meneguzzi, G.; Paulsson, M.; Sanes, J.; Timpl, R.; Yamada, K. T.; Yurchenco, P. D. *Matrix Biol.* **1994**, *14*, 209.
(12) Yurchenco, P. D.; Tsilibary, E. C.; Charonis, A. S.; Furthmayr, H. *J. Biol. Chem.* **1985**, *260*, 7636.
(13) Paulsson, M. *J. Biol. Chem.* **1988**, *263*, 5425.
(14) Ramsden, J. J. *Biopolymers* **1993**, *33*, 475.
(15) Paulsson, M.; Aumailley, M.; Deutzmann, R.; Timpl, R.; Beck, K. E. J. *Eur. J. Biochem.* **1987**, *166*, 11.
(16) Engel, J.; Furthmayr, H. *Extracell. Matrix Compon.* **1987**, *145*, 3.
(17) Chen, C. H.; Clegg, D. O.; Hansma, H. G. *Biochemistry* **1998**, *37*, 8262.
(18) Georgalis, Y.; Zouni, A.; Saenger, W. *J. Cryst. Growth* **1992**, *118*, 360.
(19) Kadima, W.; McPherson, A.; Dunn, M. F.; Jurnak, F. A. *Biophys. J.* **1990**, *57*, 125.
(20) Boyer, M.; Roy, M.-O.; Jullien, M. *J. Cryst. Growth* **1996**, *167*, 212.
(21) Lafont, S.; Veesler, S.; Astier, J.-P.; Boistelle, R. *J. Cryst. Growth* **1997**, *173*, 132.
(22) Onuma, K.; Kubota, T.; Tanaka, S.; Kanzaki, N.; Ito, A.; Tsutsui, K. *J. Phys. Chem. B* **2002**, *106*, 4318.
(23) Tanaka, S.; Ataka, M. *J. Chem. Phys.* **2002**, *117*, 3504.
(24) Verwey, E. J. W.; Overbeek, J. Th. G. *Theory of the Stability of Lyophobic Colloids*; Elsevier: Amsterdam, 1948.
(25) Pusey, P. N.; Tough, R. J. A. *Dynamic Light Scattering*; Plenum: New York, 1985.
(26) Ziman, J. M. *Models of Disorder*; Cambridge University Press: 1978.
(27) Hunter, R. J. *Foundations of Colloidal Hydrodynamics*; Clarendon: Oxford, U.K. 1989.
(28) Corti, M.; Degiorgio, V. *J. Phys. Chem.* **1981**, *85*, 711.
(29) Eberstein, W.; Georgalis, Y.; Saenger, W. *J. Cryst. Growth* **1994**, *143*, 71.
(30) Hamaker, H. C. *Physica* **1937**, *4*, 1058.
(31) Tanaka, S.; Ataka, M.; Onuma, K.; Kubota, M. *Biophys. J.* **2003**, *84*, 3299.
(32) Finet, S.; Tardieu, A. *J. Cryst. Growth* **2001**, *232*, 40.
(33) Muschol, M.; Rosenberger, F. *J. Chem. Phys.* **1995**, *103*, 10424.
(34) Petsev, D. N.; Vekilov, P. G. *Phys. Rev. Lett.* **2000**, *84*, 1339.
(35) Narayanan, J.; Liu, X. Y. *Biophys. J.* **2003**, *84*, 523.